SCIENCE CHINA
Earth Sciences

• RESEARCH PAPER •

December 2017 Vol.60 No.12:2214–2222
doi: 10.1007/s11430-017-9089-9

New insights on the origin of the basement of the Xisha Uplift, South China Sea

ZHU WeiLin[1], XIE XiNong[2], WANG ZhenFeng[3], ZHANG DaoJun[3], ZHANG ChengLi[4], CAO LiCheng[1] & SHAO Lei[1*]

[1] *State Key Laboratory of Marine Geology, Tongji University, Shanghai 200092, China;*
[2] *Key Laboratory of Tectonics and Petroleum Resources, Ministry of Education, China University of Geoscience (Wuhan), Wuhan 430074, China;*
[3] *Zhanjiang Branch, CNOOC Limited, Zhanjiang 524057, China;*
[4] *Department of Geology, Northwestern University, Xi'an 710069, China*

Received January 9, 2017; accepted July 31, 2017; published online September 1, 2017

Abstract The study of basement geochronology provides crucial insights into the tectonic evolution of oceans. However, early studies on the basement of the Xisha Uplift were constrained by limited geophysical and seismic data; Xiyong1 was the only commercial borehole drilled during the 1970s because of the huge thickness of overlying Cenozoic strata on the continental margin. Utilizing two newly-acquired basement samples from borehole XK1, we present petrological analysis and zircon uranium (U)-lead (Pb) isotope dating data in this paper that enhance our understanding of the formation and tectonic features of the Xisha Uplift basement. Results indicate that this basement is composed of Late Jurassic amphibole plagiogneisses that have an average zircon $^{206}Pb/^{238}U$ age of 152.9±1.7 Ma. However, the youngest age of these rocks, 137±1 Ma, also suggests that metamorphism termination within the Xisha basement occurred by the Early Cretaceous. These metamorphic rocks have adamellites underneath them which were formed by magmatic intrusions during the late stage of the Early Cretaceous (107.8±3.6 Ma). Thus, in contrast to the Precambrian age (bulk rubidium (Rb)-strontium (Sr) analysis, 627 Ma) suggested by previous work on the nearby Xiyong1 borehole, zircons from XK1 are likely the product of Late Mesozoic igneous activity. Late Jurassic-Early Cretaceous regional metamorphism and granitic intrusions are not confined to Xisha; rocks have also been documented from areas including the Pearl River Mouth Basin and the Nansha Islands (Spratly Islands) and thus are likely closely related to large-scale and long-lasting subduction of the paleo-Pacific plate underneath the continental margins of East Asia, perhaps the result of closure of the Meso-Tethys in the South China Sea (SCS). Controversies remain as to whether, or not, the SCS region developed initially on a uniform Precambrian-aged metamorphic crystalline basement. It is clear, however, that by this time both Mesozoic compressive subduction and Cenozoic rifting and extension had significantly modified the original basement of the SCS region.

Keywords South China Sea, Xisha Islands, Basement, Mesozoic, Zircon dating

Citation: Zhu W L, Xie X N, Wang Z F, Zhang D J, Zhang C L, Cao L C, Shao L. 2017. New insights on the origin of the basement of the Xisha Uplift, South China Sea. Science China Earth Sciences, 60: 2214–2222, doi: 10.1007/s11430-017-9089-9

1. Introduction

The South China Sea (SCS) is a unique marginal basin within the western Pacific Ocean that is located at the convergence between the Eurasian, Pacific, and Indo-Australian plates. This sea exhibits a number of distinctive tectonic characteristics and has had a complex geological history. The evolution of the SCS has been the focus of international research since the 1970s; this region is studied by an increasing number of researchers (e.g., Cullen et al., 2010; Franke et al., 2014; Kido et al., 2001; Li et al., 2014; Zhou et al., 2005), with, in particular, Ocean Drilling Program expedition 184 in 1999, and In-

* Corresponding author (email: lshao@tongji.edu.cn)

ternational Ocean Discovery Program expeditions 349, 367, and 368 in 2014 and 2017, respectively, providing important research materials and new evidence for geological studies. However, a clear understanding of the geological evolution of the SCS prior to rifting and expansion still remains elusive.

The basement of the SCS was a crucially important factor in basin formation, and is closely related to ocean evolution as well as petroleum migration and accumulation (Braitenberg et al., 2006). Since the beginning of the 1980s, a series of studies have been performed on the Cenozoic basement of the SCS, including comprehensive analyses of geophysical and seismic data. Available data on the latter, however, are mainly derived from artificial shallow depth earthquakes, while the resolution of pre-Cenozoic seismic data remains too low for analysis. In addition, the Cenozoic sediments underlying the SCS basement have been rarely drilled because of their large thickness. Taken together, these factors have led to a confused understanding of the northern SCS pre-Cenozoic basement (e.g., Liu et al., 2004; Liu and Zhan, 1994; Xie et al., 2010; Lu et al., 2011). The rocks that comprise this basement tend to get younger from west to east (Sun et al., 2014), separated by the Qionghai and Yangjiang-Yitong shoal faults (Figure 1). Previous evidence collected in the 1970s from Precambrian metamorphic rocks in the Xiyong1 borehole on Xisha Island led to the hypothesis that the northwestern region of the SCS developed on top of a Precambrian crystalline block (Wang et al., 1979); beneath the paleo-weathered crust, the SCS basement is mainly comprised of metamorphosed sedimentary rocks, including gray, grayish-green granitic gneiss and biotite plagioclase K-feldspar gneiss that have an Rubidium (Rb)-strontium (Sr) isochron age of 627 Ma. Thus, based on interpretation of joint gravity-magnet-seismic inversion data from the Xiyong1 borehole, additional possible structural layers of Precambrian basement were later identified in the western Pearl River Mouth and Qiongdongnan basins. Yue et al. (2013) suggested that the northern SCS crystalline basement might be part of the Cathaysia Craton and therefore correlated with the lower-middle Paleoproterozoic Dikou Formation in Fujian, the upper Paleoproterozoic Yunkai Group in Guangdong, and the middle Paleoproterozoic Baoban Group in Hainan. Other researchers, however, have suggested that the Xisha metamorphic crystalline basement is more likely to be an eastward extension of the Indochina Kontum Massif (Liu et al., 2011).

Although widely accepted by scholars, the age of the Precambrian crystalline Xisha Uplift basement in borehole Xiyong1 as derived from bulk Rb-Sr analysis is likely to be of no particular geological significance (Dickin, 2005). This is because, on the one hand, the rocks tested for this analysis might not have been typical orthometamorphite, while on the other, the resultant Rb-Sr isochron line was actually derived from more than one sample which generated older ages. In an earlier study, Sun (1987) expressed doubts about the accuracy of this Precambrian age and re-dated the last basement rock metamorphic event. The revised implications of this study (Sun, 1987) were that the Xisha basement formed between the Paleozoic and Mesozoic (between 627 and 96 Ma), a conclusion supported by a newly obtained 96 Ma age from K-Ar chronology. Thus, because of ongoing controversy over the age of the Xisha basement, we undertook a combination of rock slice identification and analysis of zircon uranium (U)-lead (Pb) isotopic characteristics in order to develop a more accurate understanding of Xisha basement formation time. Zircons are one kind of accessory mineral that are widely distributed in various rock types of rocks; these minerals are also very stable and are not easily modified via multicyclic sedimentation or medium metamorphism. In addition, U-Pb isotopes have the highest closure temperature of any such system, which means they present an ideal approach for evaluating the ages of metamorphic and magmatic crystallization events. Compositional and chronological studies

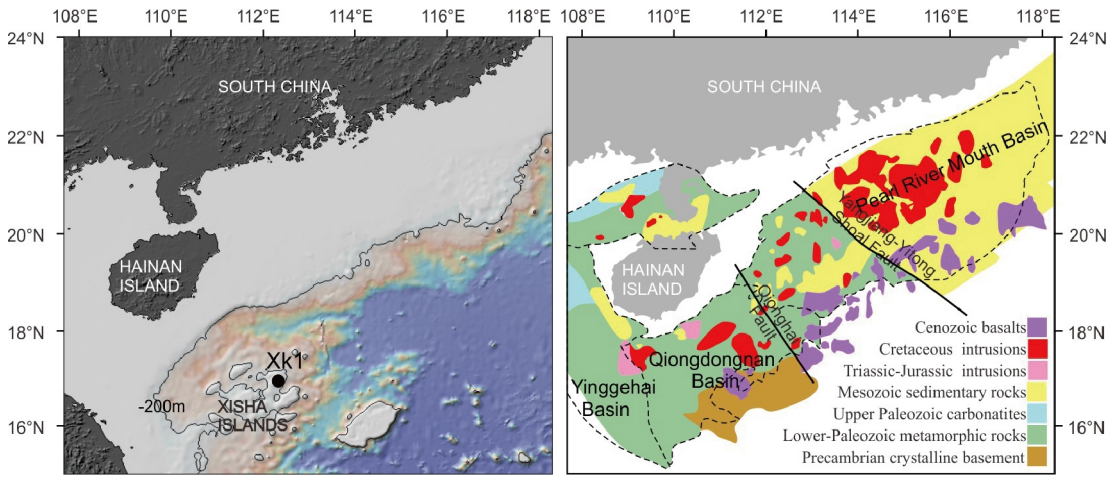

Figure 1 Maps to show the location and lithology surrounding borehole XK1 drilled into the basement of the northern SCS. Modified from Sun et al. (2014).

of the Xisha Uplift basement will enhance our understanding of the pre-Cenozoic tectonic evolution of adjacent plates of the northern SCS, and will also contribute significantly to oil and gas exploration in similar Mesozoic residual basins.

2. Geological setting

Subsequent to the opening and spreading of the Paleo-Tethys in the Early Devonian, North and South China as well as the Indochina blocks gradually drifted northwards to their present locations after separating from northeastern Gondwana (Metcalfe, 2013). Between the Triassic and the Late Cretaceous, the Sunda block and eastern Eurasia underwent extensive collision and experienced subduction of the paleo-Pacific plate which led to large-scale igneous activity along this active continental margin and strong crustal heterogeneity (Pubellier and Morley, 2014). Soon afterwards, extension and thinning of the northern SCS crust in the Early Cenozoic further altered early basement structure with the eastern continental margin subject to greater crustal extension than its western counterpart (Hayes and Nissen, 2005; Bai et al., 2015). Nevertheless, as intraplate and marginal magmatism still occurred periodically from the Middle Miocene onwards when the SCS stopped spreading (Huang et al., 2013), both the composition and structure of this original basement have been shaped by multi-stage tectonic activities. Previous seismic profiles, gravity, and magnetic interpretations suggest that the continental crust of the SCS thins both from north to south and from west to east (Wang et al., 2006), and that three distinct crustal types formed, continental, transitional, and oceanic. A series of Cenozoic rifting basins then formed from west to east on this basement, the Yinggehai, Qiongdongnan, and Pearl River Mouth basins, respectively (Figure 1).

The area studied in this work, the Xisha Islands, comprise a series of numerous islands and reefs, and are located along the northwestern continental margin of the SCS. Hainan Island and the Vietnam shelf are located to the west of the Xisha Islands, while the Xisha trough is to the north, and the SCS basin and Zhongsha Islands are to the southeast. Huang et al. (2011) reported that the crust in this area has been slightly thinned between 26 and 28 km, while a low-velocity layer (LVL) between 1 and 2 km thick as well as an average shear wave velocity between 2.0 and 2.2 km s^{-1} imply continuous deposition of carbonate during the Neogene. A prominent LVL is also present in the lower crust that has an average shear wave velocity of 3.5 km s^{-1}; this layer is thought to be correlated with the presence of anisotropic directionally-aligned minerals as well as a ductile rheological structure in the deep mantle. Lumpy, weak magnetic alternative positive and negative anomalies with low background values between −100 nT and 100 nT also dominate the Xisha-Zhongsha area; some scholars have argued that these relatively weak magnetic anomalies are indicative of a weak-magnetic metamorphic Precambrian basement, while zonally-strong anomalies are likely the result of intrusive bodies (Hao et al., 2009).

Amongst the major fault systems within our study area, the tectonic properties of the Xisha trough are of particular importance. Based on early seismic profiles and a gravity interpretation, Nissen et al. (1995) concluded that the crust of the Xisha trough thinned towards the south and had asymmetric structures on both sides. In contrast, Yao et al. (1994) argued that this trough used to be a paleosuture line while the Xisha-Zhongsha area was formerly part of the Indochina block. However, the OBH1996-IV borehole drilled across the Xisha trough suggests that both sides of this structure share similar crust and upper mantle features. Severe uplift of the Moho has also resulted in a typical extensional lift valley in this area that is thick in the middle and thin on its sides (Qiu et al., 2001). The presence of strong positive anomalies that form a striped-pattern probably implies the reverse magnetic induction of basic-ultrabasic materials or the oblique magnetization of invisible high-magnetic rock in the margin of the northern Xisha trough (Zhang et al., 2009).

3. Material and methods

Out of the four existing scientific boreholes (i.e., Xiyong1, Xiyong 2, Xichen1, and Xishi1) on the Xisha Islands, just the first (Xiyong1) was straight drilled into a 1251 m reef sequence. In contrast, borehole XK1 was drilled from an altitude of 1.5 m to a bottom depth of 1268.2 m on Shidao Island in the Xuande Atoll within the Xisha Basin between 2013 and 2014 by the Zhanjiang Branch of the China National Offshore Oil Company. The XK1 borehole also encompasses the highest core coverage percentage and shows that a 1257.52 m thick Cenozoic carbonate succession unconformably overlies Paleozoic, or even older, metamorphic rocks. Two rock samples from the basement are shown in Figure 2; these samples were taken from depths of 1258.5 m (XK1-1) and 1261.5 m (XK1-2), respectively.

The composition, concentration, proportion, texture, and structure of the dominant minerals in each sample were identified and named using a crossed-polarized light microscope.

Sample XK1-1 (from a depth of 1258.5 m) comprises dark gray amphibole plagiogneisses that mainly consists of plagioclase (46%), hornblende (11%), biotite (23%), quartz (12%), and potassium (K)-feldspar (8%), alongside a small proportion of accessory minerals such as epidote, apatite, sphene, and zircon. The grain size within this sample is also highly variable, ranging between 10 and 0.2 mm, with light-colored minerals generally tending to be larger than their dark-colored counterparts. Some feldspar grains are up to 10 mm in size and are characterized by tabular crystals, while other, dark-colored, minerals tend to be smaller than light-colored

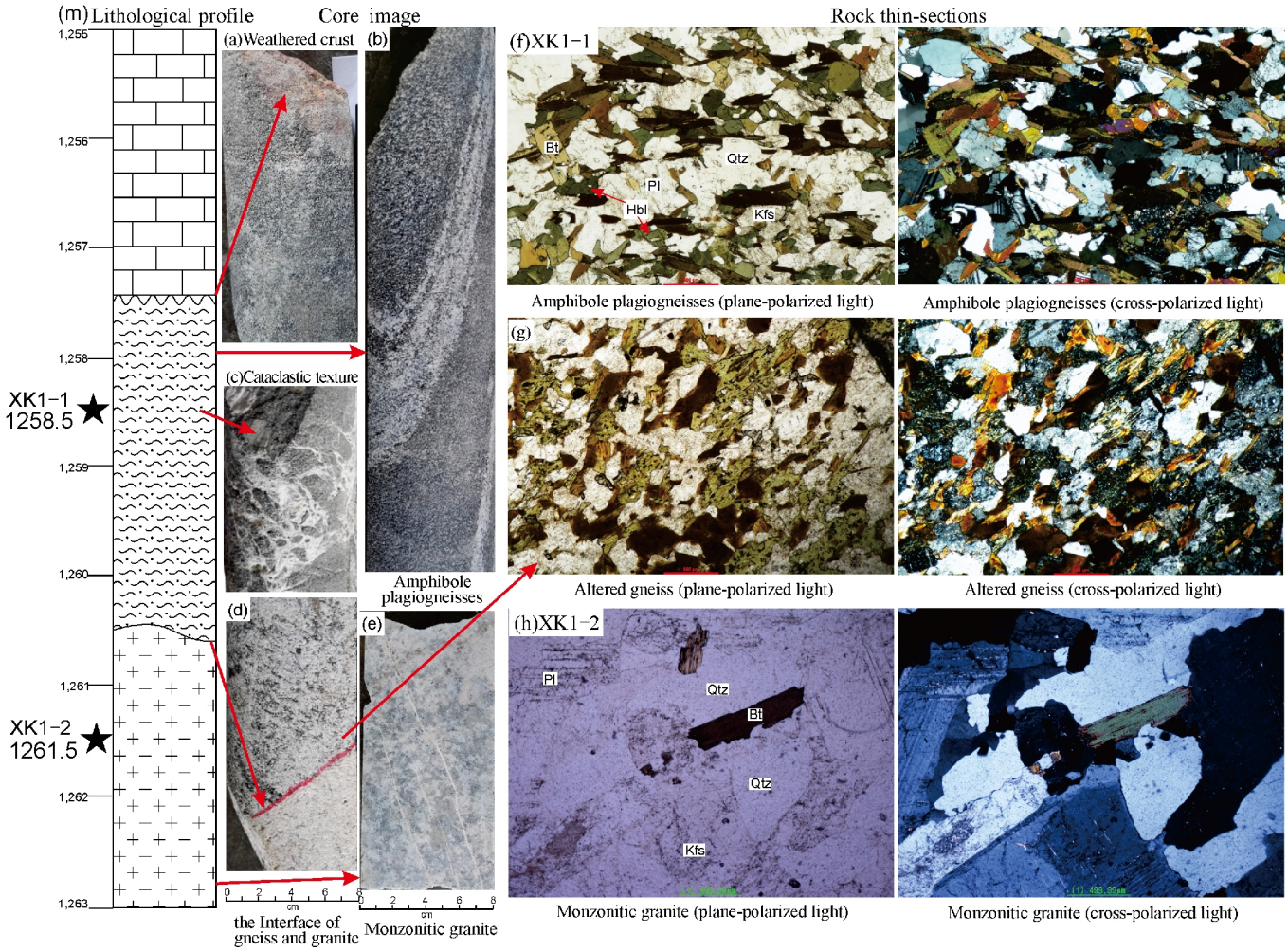

Figure 2 Lithological and petrological features of samples from borehole XK1 drilled into the Xisha Basin basement. Pl, plagioclase; Kfs, K-feldspar; Qtz, quartz; Bt, biotite; Hbl, hornblende.

ones and range in dimensions between 4 and 0.2 mm. Most minerals in this sample are preserved in their original form without secondary alteration; just one K-feldspar example is characterized by argillization and is light maroon in color because of the absorption of ferric ions. The minerals in the XK1-1 sample are also characterized by highly directional arrangements, while the presence of alternating light and dark-colored mineral-rich layers constitute a kind of medium to coarse gneiss structure (Figure 2b). Equilibrium structures between hornblendes and plagioclase at certain zonations are also evident (Figure 2f); thus, based on all these features, this rock type can be described as an amphibole plagiogneiss. Data show that this rock formed at depths between 1257.52 and 1260.52 m; an unconformable contact with crystalline limestone is seen on its top surface, weathered crust is present between the two (Figure 2a), and partial fragmentation can also be seen that was later filled with calcite veins (Figure 2c). It is also noteworthy that this amphibole plagiogneisse was obviously subject to granite intrusion at a depth of 1260.52 m; while altered gneiss is present at the contact surface, hornblende and biotite chloritization, as well as a high degree of argillization and plagioclase sericitization are also present and all minerals retain an overall directional alignment (Figure 2d and g).

Sample XK1-2 comes from depths between 1260.52 and 1262.72 m and is a light gray granite. This rock type contains large euhedral to subhedral grains that range between 20 and 5 mm in size. This sample also exhibits a typical granitic composition that essentially comprises acidic plagioclase (±22%), orthoclase (45%), and quartz (±28%), as well as a dark-colored mineral such as biotite (±5%). Accessory minerals present within XK1-2 mainly include allanite, apatite, and zircon (Figure 2e and h).

The zircon-sorting process for this study was carried out at the Hebei Province Regional Geology Minerals Investigation Research Institute. About 200 randomly chosen zircons from each sample were pasted onto double-sided adhesive tape, and were later mounted within an epoxy resin disc prior to polishing and imaging under both reflected and transmitted light. Prior to U-Pb isotopic analyses, all zircon grains

were photographed using cathodoluminescence (CL) to target their internal structures and to determine the position of microzonation. Isotopic analyses were then performed at the State Key Laboratory of Geological Processes and Mineral Resources, China University of Geoscience (Wuhan), using laser ablation inductively coupled plasma mass spectrometry (LA-ICP-MS) in a GeoLasPro 2005 LA system coupled to an Agilent 7500a ICP-MS (Liu et al., 2010). Our ablation protocol utilized a spot diameter of 32 μm at 5 Hz, while helium was used as the carrier gas to efficiently transport aerosol to the ICP-MS. We choose to laser ablate oscillatory-zoned areas of zircon crystals in all cases; each data point includes 20 s of blank signal followed by 50 s of sample signal. We inserted two zircon 91500 samples as external standards for every six sample analysis data points, and performed zircon microelement calibrations using NIST 610 glass as the external standard and silicon as the internal standard. The standard zircon GJ-1 was used as primary reference material to validate the accuracy of our analytical results, and we corrected our U-Pb raw data offline using ICPMSDataCal 7.0 (Liu et al., 2009). We corrected the measured U-Th-Pb isotopic ratio (1σ) for the common presence of Pb using Andersen's method (Andersen, 2002), while zircon U-Pb concordia plots and weighted average ages were finished using the software Isoplot (Ludwig, 2003).

4. Zircon U-Pb geochronology

Results of zircon LA-ICP-MS U-Pb isotopic dating for samples from borehole XK1 are presented in Table 1. These data show that Th/U ratios from samples XK1-1 and XK1-2 range between 0.37 and 0.88, and 0.39 and 1.01, respectively (Figure 3). Thus, taking into account oscillatory zoning features

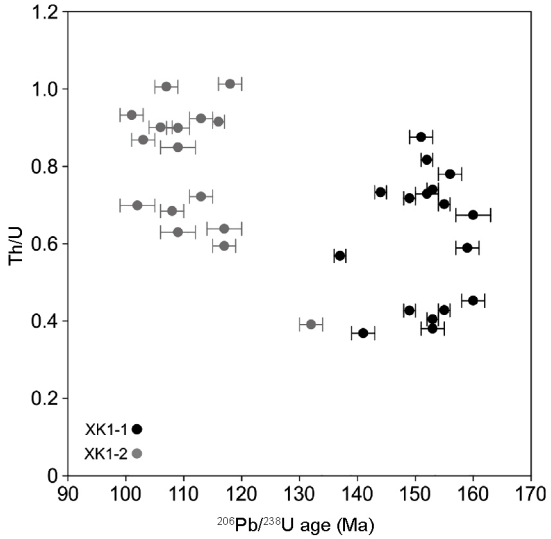

Figure 3 Summary of zircon U-Pb isotopic dates and the Th/U ratio for XK1 borehole samples from the basement of the Xisha Basin.

seen in CL images, it is likely that these zircons are the products of magma crystallization (Hoskin and Schaltegger, 2003). Our zircon U-Pb concordia plots and weighted mean age results are presented in Figure 4; these data show that 16 out of 17 analyses are concordant with a range between 160±2.5 and 137±1 Ma. In addition, 14 spots define a Late Jurassic age with a weighted mean ^{206}Pb/^{238}U age of 152.9±1.7 Ma (mean square weighted deviation, MSWD=5.5) while the other two younger spots yield Early Cretaceous ages of 160±2.5 and 137±1 Ma, respectively. Six zircon U-Th-Pb isotope dates for sample XK1-2 fall off the concordia diagram, while the remaining ten all fall within the Early Cretaceous with concordant ages between 117±2 and 101±2 Ma. Similarly, eight relatively younger zircons record a weighted mean ^{206}Pb/^{238}U crystallization age of 107.8± 3.6 Ma (MSWD=4.3) while two are older (116±1.8 and 117±2 Ma).

5. Discussion

The newly acquired amphibole plagiogneiss samples we report from the XK1 borehole drilled into the basement of the Xisha Basin overlie on Early Cretaceous granite intrusive body (107.8 Ma) that is evidence for a Late Yanshanian (Cretaceous) igneous orogeny. Large-scale Late Mesozoic tectono-magmatic events were not, however, restricted to the continental margins surrounding the SCS region (i.e., southern China, the southeastern Indochina Peninsula, and Borneo); contemporaneous granitic rocks have also been identified from oil and gas boreholes and scientific trawl surveys in the Pearl River Mouth Basin as well as in the Zhongsha and Nansha areas (Yan et al., 2014). It is also clear that this magmatic activity continued over a long period of time; previous studies have demonstrated, for example, that younger intrusive bodies are widely distributed in the Pearl River Mouth Basin while the K-Ar age of biotite granite from borehole ZHU2 (2379 m) is 70.5 Ma. In contrast, plagiogneiss samples acquired from borehole S08-18 on the Nansha Islands reveal the oldest known zircon U-Pb age of between 157.8 and 159.1 Ma (Yan et al., 2010). Although the lithological characteristics of different Late Mesozoic intrusive bodies vary from one another, we are nevertheless able to use element geochemistry to determine that an active continental margin was present in the area of the SCS before the advent of Cenozoic rifting (Yan et al., 2014). Long term compressive subduction of the paleo-Pacific slab led to large-scale landward magmatic activities along the eastern continental margin of Mesozoic Asia, as well as the development of a series of accretionary complexes at the front of this subduction zone (Metcalfe, 2013; Isozaki, 1997). At the same time, however, a great deal of ongoing controversy surrounds the exact location of subduction accretionary zones within the area of the SCS; Morley (2012) and

Table 1 Zircon crystal LA-ICP-MS U-Pb isotope dates for Xisha Basin borehole XK1 samples

Sample (run)	Content (ppm)		Th/U	Original ratio						Corrected age (Ma)					
	Th	U		$^{207}Pb/^{206}Pb$	1σ	$^{207}Pb/^{235}U$	1σ	$^{206}Pb/^{238}U$	1σ	$^{207}Pb/^{206}Pb$	1σ	$^{207}Pb/^{235}U$	1σ	$^{206}Pb/^{238}U$	1σ
XK1-1															
1	208.93	309.94	0.67	0.0550	0.0038	0.1876	0.0133	0.0252	0.0004	413	143	175	11	160	3
2	752.41	964.99	0.78	0.0491	0.0016	0.1671	0.0057	0.0246	0.0003	151	70	157	5	156	2
3	1322.34	1510.45	0.88	0.0500	0.0013	0.1632	0.0046	0.0237	0.0003	195	53	154	4	151	2
4	443.01	617.41	0.72	0.0526	0.0021	0.1682	0.0063	0.0233	0.0002	313	76	158	5	149	1
5	552.24	746.67	0.74	0.0518	0.0019	0.1725	0.0063	0.0241	0.0002	275	74	162	5	153	1
6	81.61	214.78	0.38	0.0593	0.0040	0.1884	0.0121	0.0240	0.0004	579	125	175	10	153	2
7	224.87	610.62	0.37	0.0563	0.0025	0.1721	0.0079	0.0221	0.0002	464	91	161	7	141	2
8	254.78	630.28	0.40	0.0465	0.0018	0.1540	0.0059	0.0240	0.0002	25	70	145	5	153	1
9	565.69	772.07	0.73	0.0516	0.0018	0.1612	0.0057	0.0225	0.0002	268	72	152	5	144	1
10	1361.66	2395.08	0.57	0.0508	0.0015	0.1510	0.0046	0.0214	0.0002	232	61	143	4	137	1
11	238.84	558.31	0.43	0.0510	0.0021	0.1706	0.0068	0.0243	0.0002	241	81	160	6	155	1
12	1170.73	1433.09	0.82	0.0493	0.0014	0.1630	0.0046	0.0238	0.0002	164	58	153	4	152	1
13	274.84	377.08	0.73	0.0512	0.0023	0.1669	0.0074	0.0238	0.0003	251	90	157	6	152	2
14	612.19	871.96	0.70	0.0471	0.0016	0.1583	0.0052	0.0243	0.0002	55	63	149	5	155	1
15	416.73	707.63	0.59	0.0518	0.0019	0.1783	0.0064	0.0250	0.0003	276	72	167	6	159	2
16	189.74	419.34	0.45	0.0522	0.0024	0.1799	0.0082	0.0251	0.0003	293	97	168	7	160	2
17	398.89	934.97	0.43	0.0474	0.0016	0.1546	0.0054	0.0235	0.0002	71	71	146	5	149	1
XK1-2															
16	173.31	172.33	1.01	0.0538	0.0063	0.1198	0.0125	0.0168	0.0003	363	223	115	11	107	2
17	1097.47	1847.00	0.59	0.0549	0.0018	0.1411	0.0051	0.0186	0.0003	89	89	116	6	117	2
18	72.73	113.89	0.64	0.0755	0.0084	0.1796	0.0192	0.0183	0.0004	1081	209	168	16	117	3
19	74.33	106.37	0.70	0.1057	0.0089	0.2316	0.0186	0.0166	0.0004	865	295	141	20	102	3
20	209.01	535.10	0.39	0.0681	0.0060	0.1926	0.0173	0.0207	0.0004	873	180	179	15	132	2
21	144.69	156.66	0.92	0.0611	0.0064	0.1455	0.0149	0.0176	0.0004	643	216	138	13	113	2
22	84.52	99.55	0.85	0.1222	0.0115	0.2519	0.0200	0.0171	0.0004	1989	133	228	16	109	3
23	75.27	109.95	0.68	0.0520	0.0078	0.1241	0.0194	0.0170	0.0004	286	314	119	17	108	2
24	151.51	168.20	0.90	0.0493	0.0053	0.1050	0.0115	0.0166	0.0003	160	224	101	11	106	2
25	1276.40	1394.15	0.92	0.0473	0.0017	0.1190	0.0042	0.0182	0.0002	63	70	114	4	116	1
26	191.92	213.44	0.90	0.0572	0.0054	0.1319	0.0119	0.0170	0.0003	501	193	126	11	109	2
27	163.88	161.79	1.01	0.0661	0.0057	0.1623	0.0137	0.0184	0.0004	811	168	153	12	118	2
28	83.47	115.65	0.72	0.0682	0.0072	0.1560	0.0164	0.0177	0.0004	874	213	147	14	113	2
29	124.82	133.85	0.93	0.0689	0.0081	0.1356	0.0145	0.0157	0.0004	896	215	129	13	101	2
30	87.05	100.25	0.87	0.0796	0.0097	0.1637	0.0176	0.0161	0.0004	1187	208	154	15	103	2
31	60.96	96.85	0.63	0.0750	0.0098	0.1666	0.0213	0.0170	0.0004	1068	256	156	19	109	3

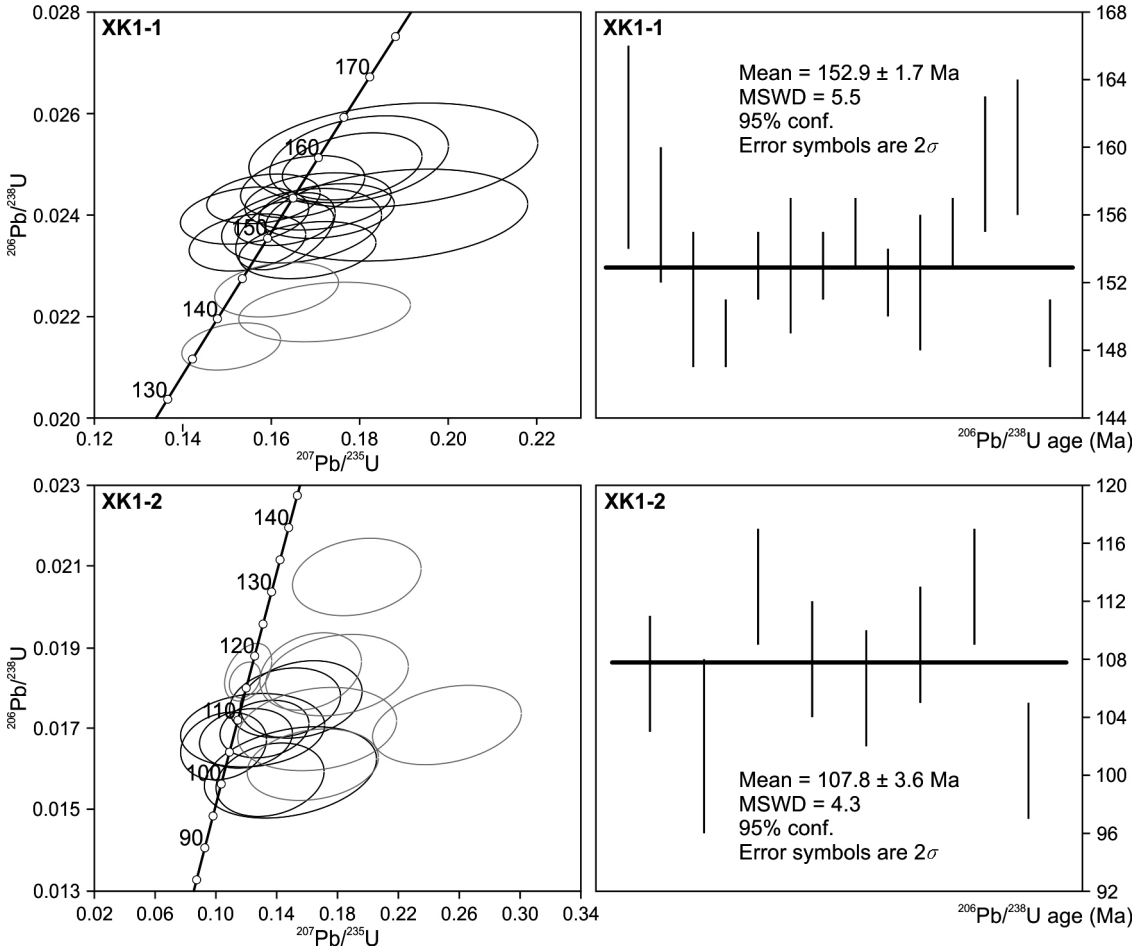

Figure 4 Zircon U-Pb concordia plots and weighted mean ages for XK1 borehole samples from the basement of the Xisha Basin.

Zahirovic et al. (2014) presented models for tectonic evolution showing that these subduction zones passed directly across the eastern Indochina Peninsula and western Borneo through coastal areas of southern China and eastern Hainan Island, while Taylor and Hayes (1983) made the alternative suggestion that the paleo-Pacific slab was subducted northwestwards underneath the north Palawan terrane and Reed Bank. Some other researchers have also focused on a segment of buried striped subduction zone that is present in the northeastern SCS beneath Cenozoic cover. This zonal segment approximately encompasses the region between NE45° and SW225° and runs from the southwestern Taiwan Basin to the Zhongsha Islands, oblique to seafloor topography and the Cenozoic tectonic stress field. In addition, the peak of gross horizontal gradient Bouguer gravity anomaly seen in this segment appears to be comparable to the Manila trench in both scale and strength, also illustrating a relatively high magnetic anomaly. All these lines of evidence likely indicate the presence of a volcanic arc related to Cenozoic subduction (Zhou et al., 2008; Li et al., 2008).

The results of this study show that while Borehole XK1 is located just 1 km from Xiyong1, the metamorphic rocks in both have been affected by a synchronous tectonic thermal event. At the same time, however, the newly acquired amphibole plagiogneisse samples from XK1 yield an average zircon crystallization age of 152.9 Ma and a minimum age of 137±1 Ma. These dates are indicative of Late Jurassic to Early Cretaceous metamorphism, and are far younger than the Precambrian Rb-Sr isotopic age (627 Ma) identified in earlier work from Xiyong1 basement samples. Indeed, even if a Precambrian crystalline basement is located underneath Hainan Island, southern China, and the Kontum massif in central Vietnam, reliable evidence from a systematic body of research is still absent with regard to the existence of a uniform ancient metamorphic basement underlying the whole SCS. Although a MSWD value of 5.5 for zircon $^{206}Pb/^{238}U$ ages from borehole XK1-1 is slightly higher than in previous work, ages are nevertheless relatively well focused at a younger, rather than Paleozoic or an even older, age. Sun et al. (2014) recently summarized a great deal of data from borehole metamorphic rock samples across the northern SCS basin and spanning the Precambrian to Paleozoic. None of the basement rock samples so far collected from boreholes (e.g., KP1-1-1 and YJ35-1-1 from the Pearl River Mouth Basin) have yielded accurate age data or led to a convincing stratigraphic analysis. For example, the two-mica plagiogneiss drilled from a

depth of 2480 m within borehole LF2-1-1 in the Pearl River Mouth Basin yielded a K-Ar isotopic age of 100 Ma (Li et al., 1998), while Mesozoic metamorphic rocks were collected from the Nansha Islands during expeditions SO23 and SO72 in the 1980s (Kudrass et al., 1986). Similarly, mica K-Ar ages obtained from garnet-mica schist, amphibolite, paragneiss, and quartz-phyllite samples are all related to a Late Jurassic to Early Cretaceous metamorphic event (i.e., between 113 and 146 Ma). Research by Fyhn et al. (2010) has also suggested that the Nansha block used to be a micro-block located on the western edge of the paleo-Pacific during the Mesozoic and did not collide with the Indochina Peninsula until the Early Cenozoic. The results of this study show that both Nansha and Xisha basements were affected by the same regional metamorphism which lasted from the Late Jurassic to the Early Cretaceous. In addition, the fact that the Zhongsha-Xisha and Nansha blocks share striking similar magnetic basement characteristics implies the presence of a single entity prior to the expansion of the SCS (Hao et al., 2009).

It is well-known that the Mesozoic SCS was characterized by an extremely complicated tectonic background and has been regarded as a zone of interaction between Tethys and paleo-Pacific domains. This region certainly underwent strong collision and suturing during the Late Mesozoic (Pichot et al., 2014; Xia and Huang, 2000; Cai, 1998; Li, 1999; Yao, 1998; Wu, 1999). Based on distribution patterns and the relative timing of strata formation, Yan and Zhou (2001) concluded that closure of the Meso-Tethys was triggered by collision between the North Palawan-Reed Bank-Nansha block and the southern Chinese continental margin in the Middle Cretaceous. Thus, metamorphic and granite ages of the Xisha basement are helpful in determining the tectonic evolution of the Meso-Tethys as well as discrepancies in crustal structure in both east-west and south-north directions along the northern continental margin of the SCS. Contemporaneous metamorphic rocks in the Pearl River Mouth Basin as well as the basement garnet K-Ar age of 102.2±1.1 Ma from borehole MZ-1 within the Chaoshan depression both indicate that an east-west trending metamorphic belt used to be present within the northern SCS during the Cretaceous. This metamorphic belt was almost certainly caused by subduction of the Meso-Tethys along the continental margin of the northern SCS; however, whether, or not, this metamorphic belt extended westward into the Red River shear zone or was pieced together alongside an oceanic basin represented by the Sumatran Woyla suture line through the Kalimantan Meratus suture line remains unclear and will require further research.

6. Conclusions

Petrographic analyses combined with zircon U-Pb isotopic dating data of samples from borehole XK1 drilled on the Xisha Islands indicate the presence of a metamorphic basement comprised of Late Jurassic amphibole plagiogneisses with zircons ages of 152.9±1.7 Ma ($^{206}Pb/^{238}U$ age), which were intruded by magmatic bodies during the Early Cretaceous (107.8±3.6 Ma). Controversy remains, however, as to whether, or not, the SCS region initially developed on top of a uniform Precambrian metamorphic crystalline basement. Corroborated by a K-Ar age for the Xiyong1 basement (Sun, 1987), we suggest that regional Late Mesozoic metamorphism that took place between 152.9 Ma and 96.3 Ma in the Xisha basement might be closely related to large-scale and long-lasting subduction of the paleo-Pacific plate underneath the continental margins of East Asia and possibly marks the closure of the Meso-Tethys within the SCS.

Acknowledgements *This study used samples and data provided by CNOOC Ltd.-Zhanjiang. Reviewers offered critical comments and suggestions, which greatly improved this work. This work was supported by the National Major Science and Technology Project (Grant No. 2017ZX05-26-005), and the National Natural Science Foundation of China (Grant Nos. 41576059 & 91128207).*

References

Andersen T. 2002. Correction of common lead in U-Pb analyses that do not report ^{204}Pb. Chem Geol, 192: 59–79

Bai Y L, Wu S G, Liu Z, Müller R D, Williams S E, Zahirovic S, Dong D D. 2015. Full-fit reconstruction of the South China Sea conjugate margins. Tectonophysics, 661: 121–135

Braitenberg C, Wienecke S, Wang Y. 2006. Basement structures from satellite-derived gravity field: South China Sea ridge. J Geophys Res, 111: B05407

Cai Q Z. 1998. A guess about remnant Tethys: Talking from the discovery of marine facies Mesozoic Paleocene at near China Sea areas (in Chinese). China Geol, 251: 39–41

Cullen A, Reemst P, Henstra G, Gozzard S, Ray A. 2010. Rifting of the South China Sea: New perspectives. Petrol Geosci, 16: 273–282

Dickin A P. 2005. Radiogenic Isotope Geology. New York: Cambridge University Press

Franke D, Savva D, Pubellier M, Steuer S, Mouly B, Auxietre J L, Meresse F, Chamot-Rooke N. 2014. The final rifting evolution in the South China Sea. Mar Pet Geol, 58: 704–720

Fyhn M B W, Pedersen S A S, Boldreel L O, Nielsen L H, Green P F, Dien P T, Huyen L T, Frei D. 2010. Palaeocene-early Eocene inversion of the Phuquoc-Kampot Som Basin: SE Asian deformation associated with the suturing of Luconia. J Geol Soc, 167: 281–295

Hao T Y, Xu Y, Zhao B M, Zhang Y J, Peng L L. 2009. Geophysical research on distribution features of magnetic basements in the South China Sea. Chin J Geophys, 52: 2763–2774

Hayes D E, Nissen S S. 2005. The South China sea margins: Implications for rifting contrasts. Earth Planet Sci Lett, 237: 601–616

Hoskin P W O, schaltegger U. 2003. The composition of zircon and igneous and metamorphic petrogenesis. Rev Mineral Geochem, 53: 27–62

Huang H B, Qiu X L, Xu Y, Zeng G P. 2011. Crustal structure beneath the Xisha Islands of the South China Sea simulated by the teleseismic receiver function method (in Chinese). Chin J Geophys, 54: 2788–2798

Huang X L, Niu Y, Xu Y G, Ma J L, Qiu H N, Zhong J W. 2013. Geochronology and geochemistry of Cenozoic basalts from eastern Guangdong, SE China: Constraints on the lithosphere evolution beneath the northern

margin of the South China Sea. Contrib Mineral Petrol, 165: 437–455
Isozaki Y. 1997. Jurassic accretion tectonics of Japan. Isl Arc, 6: 25–51
Kido Y, Suyehiro K, Kinoshita H. 2001. Rifting to spreading process along the northern continental margin of the South China Sea. Mar Geophys Res, 22: 1–15
Kudrass H R, Wiedicke M, Cepek P, Kreuzer H, Müller P. 1986. Mesozoic and Cainozoic rocks dredged from the South China Sea (Reed Bank area) and Sulu Sea and their significance for plate-tectonic reconstructions. Mar Pet Geol, 3: 19–30
Li C F, Xu X, Lin J, Sun Z, Zhu J, Yao Y, Zhao X, Liu Q, Kulhanek D K, Wang J, Song T, Zhao J, Qiu N, Guan Y, Zhou Z, Williams T, Bao R, Briais A, Brown E A, Chen Y, Clift P D, Colwell F S, Dadd K A, Ding W, Almeida I H, Huang X L, Hyun S, Jiang T, Koppers A A P, Li Q, Liu C, Liu Z, Nagai R H, Peleo-Alampay A, Su X, Tejada M L G, Trinh H S, Yeh Y C, Zhang C, Zhang F, Zhang G L. 2014. Ages and magnetic structures of the South China Sea constrained by deep tow magnetic surveys and IODP Expedition 349. Geochem Geophys Geosyst, 15: 4958–4983
Li C F, Zhou Z, Hao H, Chen H, Wang J, Chen B, Wu J. 2008. Late Mesozoic tectonic structure and evolution along the present-day northeastern South China Sea continental margin. J Asian Earth Sci, 31: 546–561
Li J B. 1999. The migration and collision of South China Sea Geological system. In: Xu D Y, ed. Marine Geology and Paleoceanography (in Chinese). Beijing: The Proceedings of the 30th International Geological Congress. 13: 24–34
Li P L, Liang H X, Dai Y D. 1998. Exploration perspective of basement hydrocarbon accumulations in the Pearl River Mouth basin (in Chinese). China Offshore Oil Gas Geol, 12: 361–369
Liu H L, Yan P, Zhang B Y, Qiu X L, Xia B. 2004. Basement of pre-Cenozoic South China Sea and tectonic domain of eastern Tethys (in Chinese). Mar Geol Quat Geol, 24: 15–28
Liu H L, Zheng H B, Wang Y L, Lin Q J, Wu C H, Zhao M S, Du Y K. 2011. Basement of the South China Sea Area: Tracing the Tethyan Realm. Acta Geol Sin-Engl Ed, 85: 637–655
Liu Y S, Gao S, Hu Z C, Gao C G, Zong K Q, Wang D B. 2009. Continental and oceanic crust recycling-induced melt-peridotite interactions in the trans-north China orogen: U-Pb dating, Hf isotopes and trace elements in zircons from mantle xenoliths. J Petrol, 51: 537–571
Liu Y S, Hu Z C, Zong K Q, Gao C G, Gao S, Xu J, Chen H H. 2010. Reappraisement and refinement of zircon U-Pb isotope and trace element analyses by LA-ICP-MS. Chin Sci Bull, 55: 1535–1546
Liu Y X, Zhan W H. 1994. Basic outline and tectonic evolution of the metamorphic basement in the South China Sea (in Chinese). Geology Anhui, 4: 82–89
Lu B L, Wang P J, Zhang G C, Zhang B, Sun X M, Li W Z, Lang Y Q. 2011. Basement structures of an epicontinental basin in the northern South China Sea and their significance in petroleum prospecting (in Chinese). Acta Petrol Sin, 32: 580–587
Ludwig K R. 2003. User's manual for isoplot 3.00: A geochronological toolkit for microsoft excel. Berkeley: Berkeley Geochronology Center
Metcalfe I. 2013. Gondwana dispersion and Asian accretion: Tectonic and palaeogeographic evolution of eastern Tethys. J Asian Earth Sci, 66: 1–33
Morley C K. 2012. Late Cretaceous-Early Palaeogene tectonic development of SE Asia. Earth-Sci Rev, 115: 37–75
Nissen S S, Hayes D E, Bochu Y, Zeng W, Chen Y, Nu X. 1995. Gravity, heat flow, and seismic constraints on the processes of crustal extension: Northern margin of the South China Sea. J Geophys Res, 100: 22447–22483
Pichot T, Delescluse M, Chamot-Rooke N, Pubellier M, Qiu Y, Meresse F, Sun G, Savva D, Wong K P, Watremez L, Auxiètre J L. 2014. Deep crustal structure of the conjugate margins of the SW South China Sea from wide-angle refraction seismic data. Mar Pet Geol, 58: 627–643
Pubellier M, Morley C K. 2014. The basins of Sundaland (SE Asia): Evolution and boundary conditions. Mar Pet Geol, 58: 555–578
Qiu X L, Ye S Y, Wu S M, Shi X B, Zhou D, Xia K Y, Flueh E R. 2001. Crustal structure across the Xisha Trough, northwestern South China Sea. Tectonophysics, 341: 179–193
Sun J S. 1987. A discussion on the formation age of the Xisha basement (in Chinese). Mar Geol Quat Geol, 7: 5–6
Sun X M, Zhang X Q, Zhang G C, Lu B L, Yue J P, Zhang B. 2014. Texture and tectonic attribute of Cenozoic basin basement in the northern South China Sea. Sci China Earth Sci, 57: 1199–1211
Taylor B, Hayes D E. 1983. Origin and history of the South China Sea basin. In: Hayes D E, ed. The Tectonic and Geologic Evolution of Southeast Asian Seas and Islands: Part 2. Washington DC: American Geophysical Union. 23–56
Wang C Y, He X X, Qiu S Y. 1979. A preliminary study on foraminiferal assemblages of well 1 Xiyong, Xisha Islands and their coral reef formation (in Chinese). Petrol Geol Exper, 7: 23–38
Wang T K, Chen M K, Lee C S, Xia K. 2006. Seismic imaging of the transitional crust across the northeastern margin of the South China Sea. Tectonophysics, 412: 237–254
Wu H R. 1999. The implications of radiolaria-bearing siliceous rocks to the paleogeography of South China (in Chinese). J Palaeogeo, 1: 28–34
Xia K Y, Huang C L. 2000. The discovery of sediment basin of Mesozoic Tethyan and prospect of finding Mesozoic oil-gas-bearing basins in South China Sea (in Chinese). Geosci Front, 7: 227–238
Xie J L, Yu H Z, Tang L M, Fu J J, Wu J Y. 2010. Basement property and basin type of Cenozoic South China Sea sediment (in Chinese). Marin Orig Petrl Geol, 15: 35–47
Yan J X, Zhou D. 2001. The study of tectonic evolution of Meso-Tethys at the northern margin of the South China Sea area (in Chinese). Mar Geol Quat Geol, 21: 51–56
Yan Q S, Shi X F, Castillo P R. 2014. The late Mesozoic-Cenozoic tectonic evolution of the South China Sea: A petrologic perspective. J Asian Earth Sci, 85: 178–201
Yan Q S, Shi X F, Liu J H, Wang K S, Bu W R. 2010. Petrology and geochemistry of Mesozoic granitic rocks from the Nansha micro-block, the South China Sea: Constraints on the basement nature. J Asian Earth Sci, 37: 130–139
Yao B C. 1998. The crustal structure and tectonic significance of the north margin of the South China Sea (in Chinese). Marin Geol Quat Geol, 18: 1–16
Yao B C, Zeng W J, Chen Y Z, Zhang X L. 1994. Xisha trough of the South China Sea, a paleo-suture. Marin Geol Quat Geol, 14: 1–10
Yue J P, Zhang Y, Shen H L, You L, Lu B L, Wang P J. 2013. Restraint of geologic feature of South China continental margin to basin basement of northern South China Sea (in Chinese). Acta Petrol Sin, 34: 120–128
Zahirovic S, Seton M, Müller R D. 2014. The Cretaceous and Cenozoic tectonic evolution of Southeast Asia. Solid Earth, 5: 227–273
Zhang Y J, Liu Z J, Zhao B M. 2009. Geophysical understanding about the positive magnetic anomaly zone of Xisha trough. Prog Geophys, 24: 1987–1994
Zhou D, Sun Z, Chen H Z, Xu H H, Wang W Y, Pang X, Cai D S, Hu D K. 2008. Mesozoic paleogeography and tectonic evolution of South China Sea and adjacent areas in the context of Tethyan and Paleo-Pacific interconnections. Isl Arc, 17: 186–207
Zhou D, Liu H L, Chen H Z. 2005. Mesozoic-Cenozoic magmatism in southern South China Sea and its surrounding areas and its implications to tectonics (in Chinese). Geotect Metal, 29: 354–363